

Accepted by the PASP

Establishing Visible Interferometer System Responses: Resolved and Unresolved Calibrators

Gerard T. van Belle

Michelson Science Center, California Institute of Technology, Pasadena, CA 91125

gerard@ipac.caltech.edu

and

Gerald van Belle

Department of Biostatistics, University of Washington, Seattle, WA 98195-7232

vanbelle@seanet.com

ABSTRACT

The propagation of errors through the uniform disk visibility function is examined. Implications of those errors upon measures of absolute visibility through optical and near-infrared interferometers are considered within the context of using calibration stars to establish system visibilities for these instruments. We suggest a simple ratio test to establish empirically whether or not the measured visibilities produced by such an instrument are relative (errors dominated by calibrator angular size prediction error) or absolute (errors dominated by measurement error).

Subject headings: interferometry: infrared

1. Introduction

Visible and near-infrared interferometers are powerful tools for measuring the minute angular sizes of nearby stars. However, establishing absolute system responses in the presence of atmospheric turbulence and instrument imperfections is a challenging proposition that requires careful attention to detail when constructing an observational approach.

For two-element interferometers that are now commonly in use, the principal measured quantity is the visibility, V , which is simply a characterization of the contrast found in the observed interference fringe and can range from 0 to 1. In practice, interferometers that lock onto and track fringes through temporally modulating servo loops tend to measure V^2 rather than just V . A detailed discussion of fringe visibility estimators can be found in Colavita (1999).

For individual stars, the observed V^2 will decrease from unity as the source becomes resolved to the instrument, and also as the response of the instrument and atmosphere through which it observes departs for an idealized system. A common approach to account for the system response (a combination of the atmospheric and instrumental responses) is to interleave observations of calibration stars with observations of the star of interest. If the system visibility V^2_{system} is established with calibration sources, a target star’s absolute V^2 is then easily derived from the measured V^2 :

$$V^2_{normalized}(target) = \frac{V^2_{measured}(target)}{V^2_{system}} \quad (1)$$

Calibration sources are stars which have some sort of *a priori* knowledge of their angular size, and as a result, their expected values for $V^2_{predicted}$ can be predicted. Thus, from the calibrator’s measured values for $V^2_{measured}$, the system visibility V^2_{system} that characterizes the atmospheric and instrumental performance degradations is simply:

$$V^2_{system} = \frac{V^2_{measured}(calibrator)}{V^2_{predicted}(calibrator)} \quad (2)$$

It is important to note that, as is apparent from the practice of using the system visibility found in Equation 2 in Equation 1, the system visibility needs to be constant when observing both the target star and the calibration star. This consideration is significant when such objects are of differing brightness, are located in different portions of the sky, subject to varying weather conditions, or are widely separated in time. Insofar that no two stars will be of exactly the same brightness, the instrument will be required to have some measure of dynamic range in this regard; for the purposes of this investigation, we will assume all of the relevant data are properly collected within the range of constant system visibility.

For some of the sources considered for use as calibrators, angular sizes have actually been measured. However, for most of the sources considered as calibrators, some sort of indirect estimation technique needs to be employed. These techniques include angular size estimation from distance and linear size (with the second quantity often being inferred from some proxy such as spectral type), blackbody fitting, R-I and V-K proxies (Mozurkewich et al. 1991; di Benedetto 1993; van Belle 1999), and spectrophotometric fits (Blackwell & Lynas-Gray 1994; Cohen et al. 1996).

For unbiased results, it is preferred to utilize calibration sources that are ‘unresolved’ to the interferometer. A source is considered to be unresolved when the errors in V^2_{system} are dominated by the measurement error and not the prediction error ($(\sigma_{V^2})_{measured} > (\sigma_{V^2})_{predicted}$). For such a calibrator, biases in the angular size estimation technique - known or unknown - are masked by the measurement process. This is due the interferometer’s insensitivity to the unresolved calibrator’s angular size, and as such, this technique is insensitive to estimation technique biases. In the limit that the instrument performance is linear between target and calibration sources, the resultant calibration thus is considered to be an *absolute calibration* of the system visibility V^2_{system} . This approach is documented in the literature for many interferometers, including the Mark III (Mozurkewich et al. 1991), IRMA (Dyck, Benson, & Ridgway 1993), IOTA (Dyck, Benson, van Belle, & Ridgway 1996), and PTI (van Belle et al. 1999). Additionally, as we shall see in §3, this approach avoids the regime where the separate Taylor series bias due to non-linearity in the error propagation technique becomes significant as well.

Another approach seen with some regularity is the establishment of system V^2_{system} through use of resolved calibrators. In the case where instrumental limitations (typically limited sensitivity) preclude the use of an unresolved calibrator, investigators have utilized calibration sources that are resolved to establish instrument system visibilities. The strength of this approach is that resolved calibrators are typically associated with stars of greater brightness, and as a result, greater signal-to-noise is achieved in observing the calibration sources.

The weakness of this approach is that it establishes only a *relative calibration* for the measurement, and any biases inherent in the original size estimation of the calibration source propagate into the final visibility measured for the target source, albeit with additional uncertainty due to measurement error in $V^2_{measured}$. Relative V^2 measures, when properly used, are useful quantities for certain investigations - for example, the examination of the shape of a rotationally distorted star (Domiciano de Souza et al. 2003) - but are inappropriate to use as absolute values to establish quantities such as stellar linear size or effective temperature.

2. The Visibility Function and Angular Size Estimation Bias

The projections of stellar disks upon the sky are clearly not true ‘uniform disks’ (see Hajian et al. (1998) and references therein), having varying brightness from the center to the edge of their disks. However, for most stars, characterization of them as uniform disks is a reasonable approximation, and one which will lend itself to a mathematical examination

in §2.1.

A uniform disk as viewed by an interferometer exhibits a visibility function w given by:

$$V(x)^2 = w(x) = \left(\frac{2J_1(x)}{x} \right)^2 = \left(\frac{2J_1(\pi\theta B/\lambda)}{\pi\theta B/\lambda} \right)^2 \quad (3)$$

where x is the spatial frequency, and a function of projected baseline B , source angular size θ , and observational wavelength λ : $x = \pi\theta B/\lambda$ (Airy 1835; Born & Wolf 1980).

Since we will be utilizing calibration sources with predicted angular sizes θ , it is of great utility to examine the impact that errors (and potentially size estimation biases) have upon our expected values for calibration source $V^2_{predicted}$.

2.1. Uniform Disk Visibility Error Propagation

Since $w = w(\theta, B, \lambda)$, a routine propagation of errors through Equation 3 gives:

$$\sigma_w^2 = \left(\frac{\partial w}{\partial \theta} \right)^2 \sigma_\theta^2 + \left(\frac{\partial w}{\partial B} \right)^2 \sigma_B^2 + \left(\frac{\partial w}{\partial \lambda} \right)^2 \sigma_\lambda^2 + \text{cov}(\theta, B, \lambda) \quad (4)$$

with the covariance terms for this discussion expected to be zero (we will reexamine the higher order terms of Equation 4 in §3.) For evaluation of Equation 4, it is useful to employ the *jinc*(x) function, which is defined in Bracewell (2000), and its first derivative given as

$$jinc(x) = \frac{J_1(x)}{x} \text{ and } jinc'(x) = -\frac{J_2(x)}{x}. \quad (5)$$

Using the chain rule on Equations 3 and 4

$$\frac{\partial w}{\partial x} = \frac{\partial}{\partial x} \left[\left(\frac{2J_1(x)}{x} \right)^2 \right] = \frac{\partial}{\partial x} 4jinc(x)^2 = 8jinc(x)jinc'(x) = -\frac{8J_1(x)J_2(x)}{x^2} \quad (6)$$

Equation 4 can be rewritten as:

$$\sigma_w^2 = \left[-\frac{8J_1(x)J_2(x)}{x^2} \right]^2 \left[\left[\frac{\pi B}{\lambda} \right]^2 \sigma_\theta^2 + \left[\frac{\pi\theta}{\lambda} \right]^2 \sigma_B^2 + \left[-\frac{\pi B\theta}{\lambda^2} \right]^2 \sigma_\lambda^2 \right] \quad (7)$$

$$= \left[\frac{8J_1(x)J_2(x)}{x} \right]^2 \left[\left(\frac{\sigma_\theta}{\theta} \right)^2 + \left(\frac{\sigma_B}{B} \right)^2 + \left(\frac{\sigma_\lambda}{\lambda} \right)^2 \right] \quad (8)$$

In the limit that the calibrator size prediction fractional errors dominate ($\sigma_\theta/\theta \gg \sigma_B/B, \sigma_\lambda/\lambda$), we have

$$(\sigma_{V^2})_{predicted} = \sigma_w = \left[\frac{8J_1(x)J_2(x)}{x} \right] \left[\frac{\sigma_\theta}{\theta} \right] \quad (9)$$

This error propagates in quadrature back to our estimate of the system visibility in Equation 2 along with any measurement error, $(\sigma_{V^2})_{measured}$.

For consideration of $(\sigma_{V^2})_{measured}$, it is very important to not only establish the measurement scatter of a single V^2 sampling event, but to empirically establish the night-to-night measurement error found in V^2 measurements. An excellent example of such a characterization is the examination of the final V^2 residuals in the binary star fit of ι Pegasi found in Boden et al. (1999).

2.2. Absolute versus Relative Ratio Test

We may use Equations 8 and 9 to explore the impact of calibrator size prediction error σ_θ upon the system visibility error $(\sigma_{V^2})_{predicted}$. Our test case will be as follows: a 330-m baseline with a $\sigma_B = 1$ -cm error in its knowledge of projection upon the sky (which will be the product of geometry knowledge errors and timing errors, but still is a generous error bar for this term); a $\sigma_\lambda = 0.01 \mu\text{m}$ error in the knowledge of the operational wavelength, $\lambda = 2.15 \mu\text{m}$; and a 5% prediction error σ_θ in the angular size estimate for an individual calibrator. This test case is fairly representative of the current parameters of interest for the CHARA Array (ten Brummelaar et al. 2005).

For a range of angular sizes, the predicted V^2 value for the calibrator is plotted in Figure 1. As the star passes 0.690 mas, already V^2 has fallen below 50%, and drops to zero beyond 1.500 mas. Also plotted in Figure 1 on the righthand axis is a rough expectation of number of detected photons N for the CHARA Array for a G2V star, following the relationship detailed in van Belle (1999) between $V - K$ and angular size (noting that the estimate of system throughput may be inaccurate but only scales the results herein). For our hypothetical G2V star we have $V - K = 1.5$ (Bessell & Brett 1988). The predicted V^2 error derived from those values for the three error terms in Equation 8 is shown in Figure 2. We may also estimate our signal-to-noise as being proportional to $N^2 V^2$ in the read noise limited regime (the usual operational case for near-infrared interferometers) (Colavita 1999), although we note that a similar analysis we have executed for NV^2 gives results similar to those presented in this section and the next. (This latter case corresponds to photon noise-limited operations (Mozurkewich et al. 1991) in the low photon limit, as can be the case for visible interferometers.) A plot of this is shown in Figure 3, which is effectively is the product of the solid line and the dotted line squared seen in Figure 1.

A way to illustrate this point is to examine the ratio r of V^2 measurement error

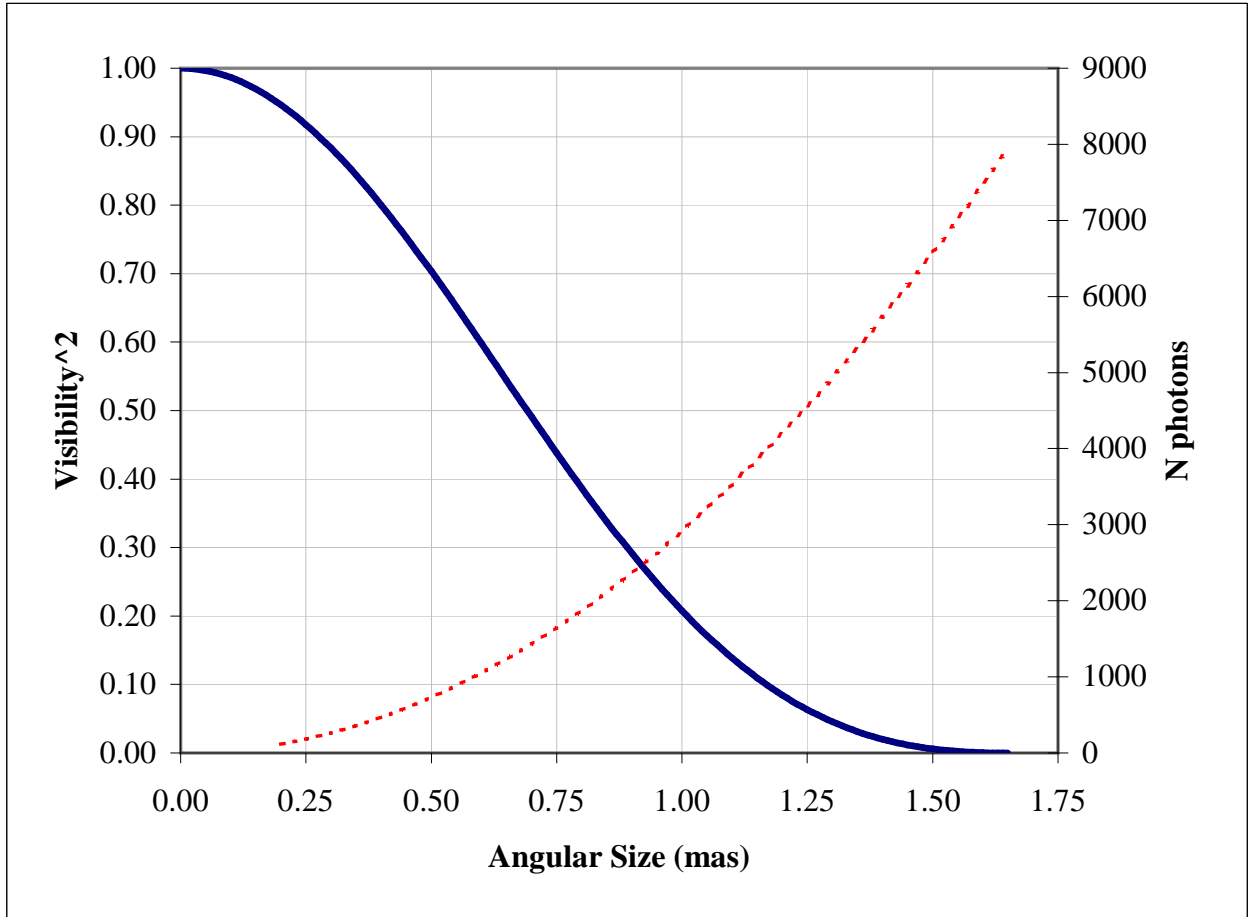


Fig. 1.— V^2 for uniform disk stars as viewed by the CHARA Array, with a 330-m baseline and a K_s bandpass. Also shown on the right vertical axis with a red dotted line is detected photon count N , assuming a G2V calibration source, a 0.001 ms integration time per sample, 1-m diameter aperture, and 4% throughput.

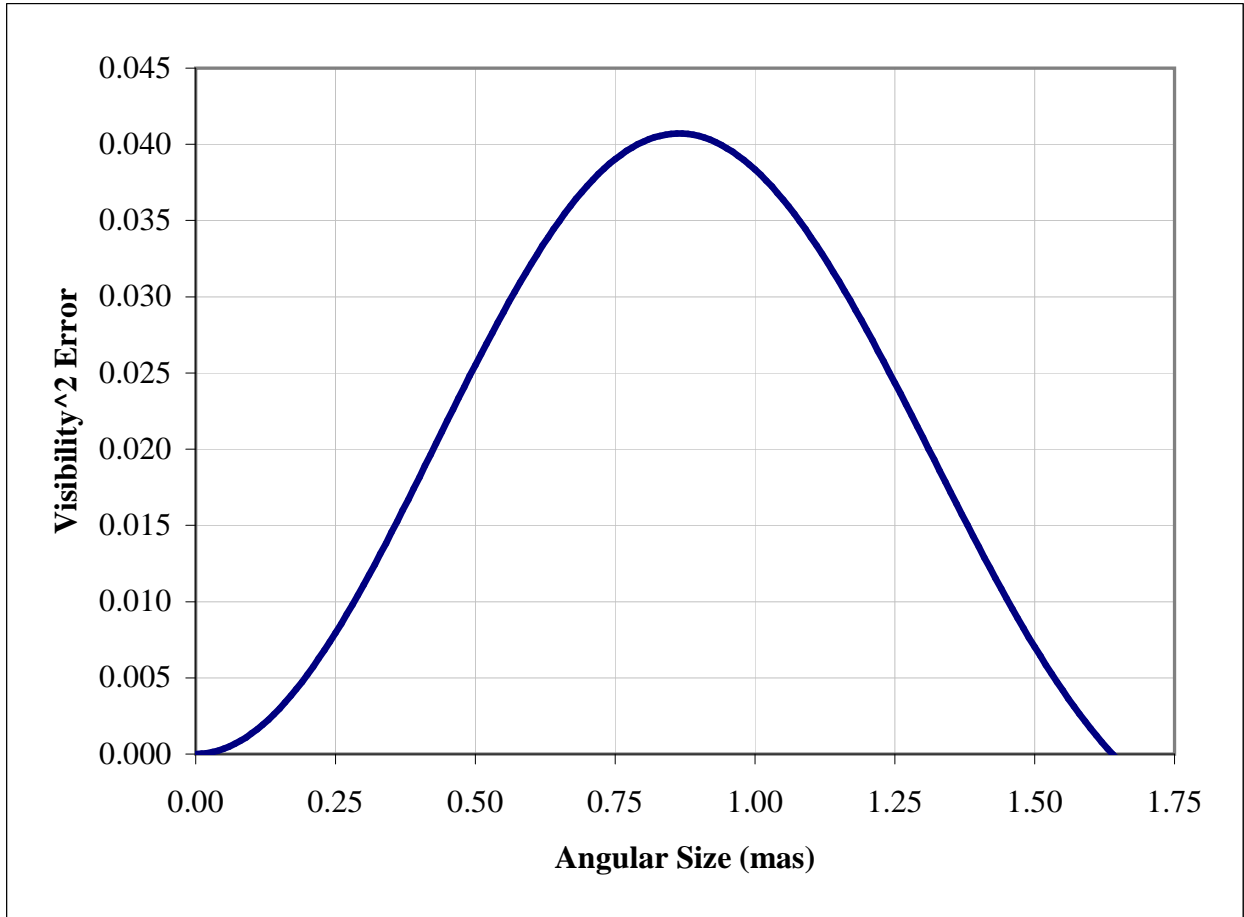


Fig. 2.— Calibrator V^2 prediction error $(\sigma_{V^2})_{predicted}$ propagated from an assumed 5% uncertainty in calibrator angular size, **not** accounting for measurement error.

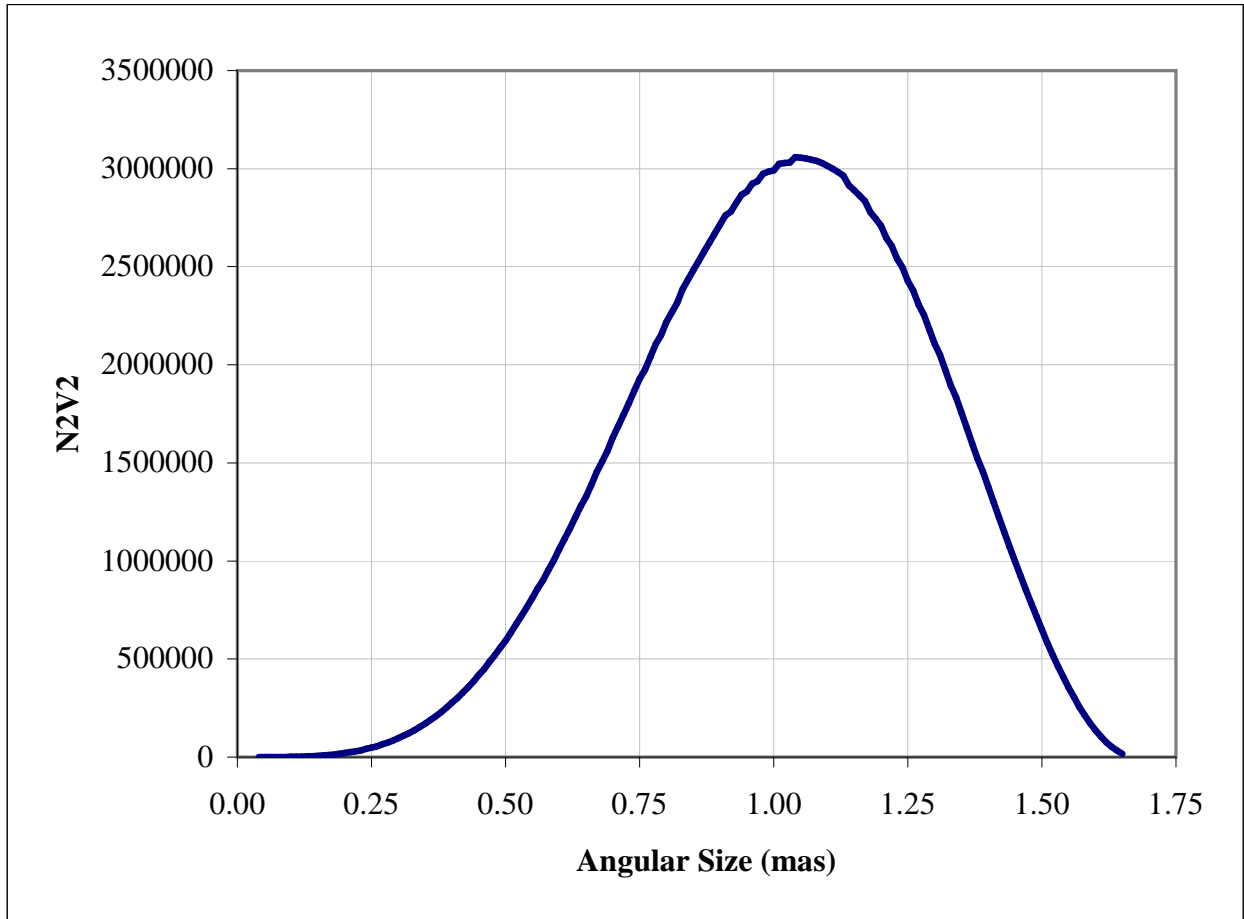


Fig. 3.— Signal-to-noise (N^2V^2) for our G2V source as a function of calibrator angular size.

$(\sigma_{V^2})_{measured}$ to calibrator V^2 prediction error $(\sigma_{V^2})_{predicted}$, as is seen in Figure 4:

$$r = \frac{(\sigma_{V^2})_{measured}}{(\sigma_{V^2})_{predicted}} \quad (10)$$

The range of angular sizes where r dips below 1.0 indicates where $(\sigma_{V^2})_{predicted}$ is a significant, if not the dominant, contribution to the V^2 measurement error. Equation 10 (with the denominator as provided by Equation 8 or 9) is a straightforward indicator of the interferometer operational regime as determined by the choice of calibrator: for $r < 1$, it is relative, and for $r > 1$, it is absolute.

It is interesting to note that Figure 4 indicates a second regime of absolute calibrator sizes for our example case, that of the ‘superresolved’ sources in the range of $\theta > 1.35$ mas. Simply put, it is in this regime that the V^2 function has once again flattened out (see Figure 1) and uncertainty in θ does little to impact $V^2_{predicted}$ for the calibrator. Unfortunately, it is in this range that the signal-to-noise is rapidly dropping to zero, as seen already in Figure 3. Also, as we will see in §3, this regime is problematic due to bias in the error propagation technique.

2.3. A Merit Function and its Evaluation

As a useful metric of ‘calibrator goodness’, we propose a merit function equal to the ratio of signal-to-noise to system visibility error:

$$m = \frac{N^2 V^2}{\sigma_{V^2}} \quad (11)$$

In the real world case, V^2 measurement error $(\sigma_{V^2})_{measured}$ also affects our measures of the system visibility. The resultant system visibility error is computed from the measurement error and the calibrator V^2 prediction error, added in quadrature:

$$\sigma_{V^2}^2 = (\sigma_{V^2})_{measured}^2 + (\sigma_{V^2})_{predicted}^2 \quad (12)$$

and applied to our merit function. The merit function incorporating the measurement error and calibrator size prediction error is plotted in Figure 5, for the case where the V^2 measurement errors are assumed to be at the 2% level.

Of interest in our CHARA Array example are the angular sizes beyond ~ 0.450 mas, where the merit function changes slope, peaks, and descends. It is at those angular sizes ($\theta > 0.450$ mas) that the contribution to the merit function transitions from V^2 measurement error $(\sigma_{V^2})_{measured}$ being dominant to calibrator V^2 prediction error $(\sigma_{V^2})_{predicted}$ becoming

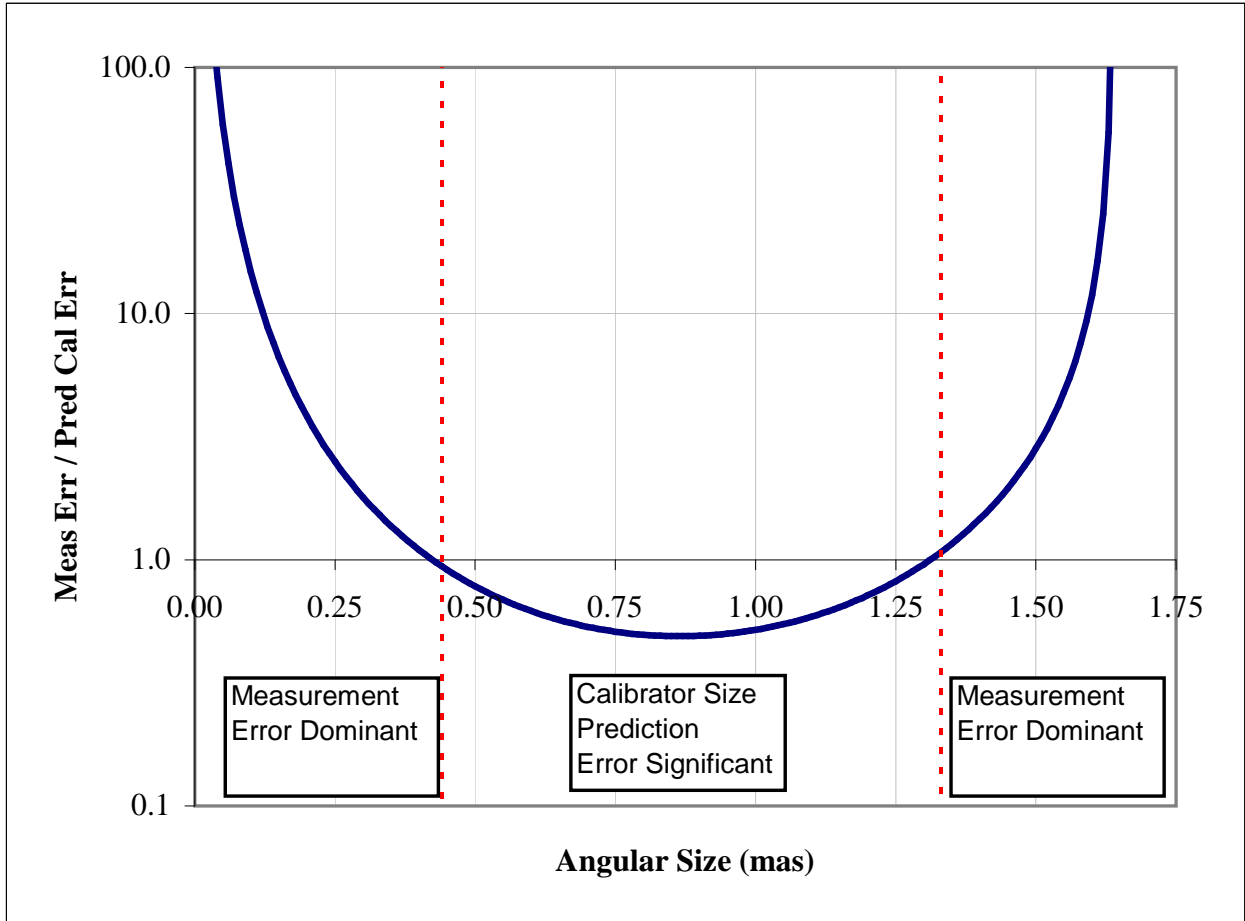


Fig. 4.— From Equation 10, the ratio of an assumed 2% V^2 measurement error to the V^2 error due to calibrator size prediction error of 5%, as a function of expected calibrator size. Note the regime between the red dotted lines, $0.45 < \theta < 1.35$ mas, where the $(\sigma_{V^2})_{predicted}$ has a significant impact upon the final errors.

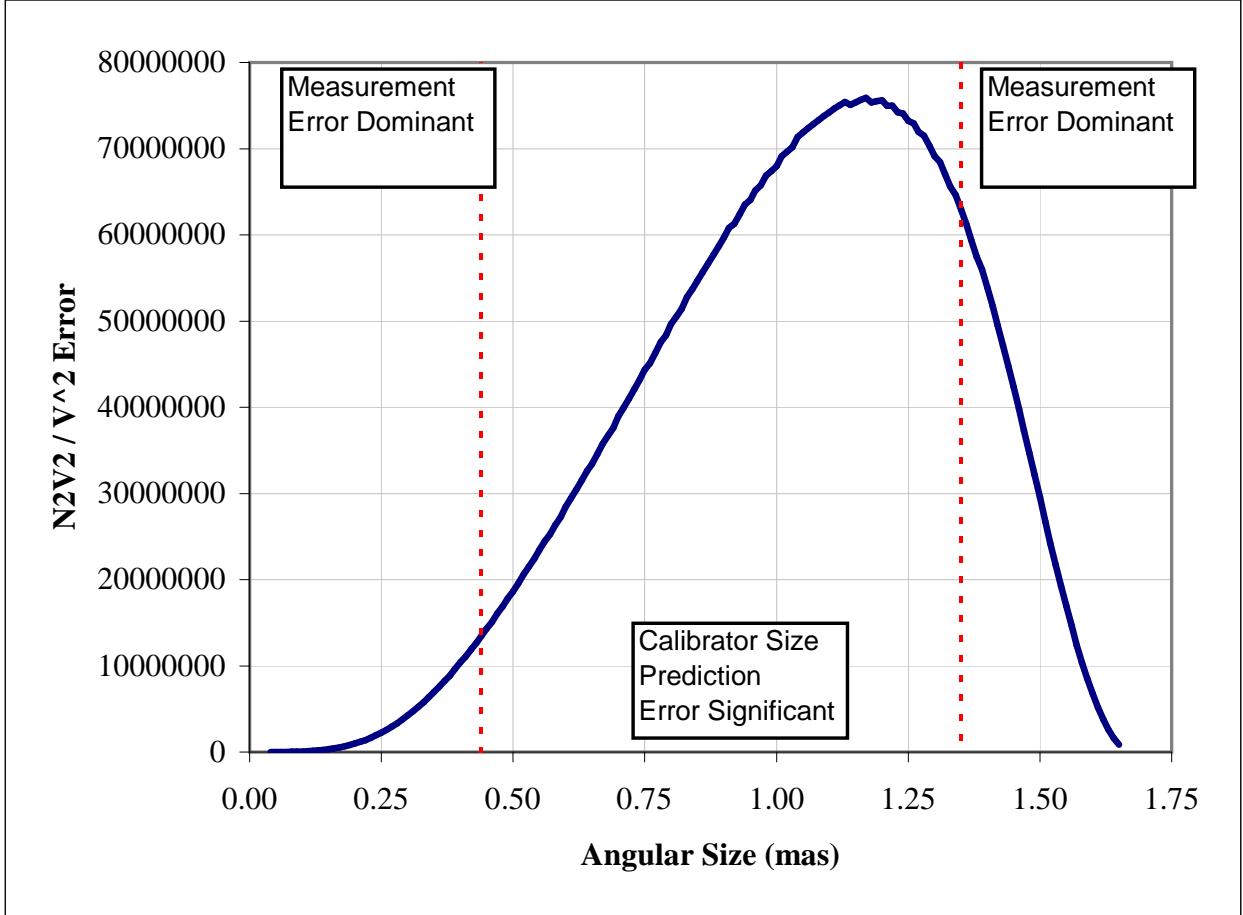


Fig. 5.— Full calibrator merit function, N^2V^2/σ_{V^2} , propagated from an assumed 5% uncertainty in calibrator angular size, and including an putative 2% V^2 measurement error. The regime to the left of the red dotted line (for this example case, $0 < \theta < 0.45$ mas) has measurement error as the dominant contribution to the merit function.

significant and then dominant. This regime is of particular interest: if the technique being employed for calibrator V^2 prediction is subject to a systematic size estimation bias due to an imperfection in the predictive technique, that bias will begin to significantly affect the inferred V^2 values for calibrators in excess of the size, despite their apparent greater ‘merit’ indicated by Equation 11. For calibrators short of this point, any systematic size estimation biases in the size prediction (and resultant V^2 prediction) will be masked by the calibrator’s point-like nature for the interferometer system.

2.4. Stellar Angular Size Prediction Bias Example: The Blackbody Case

If we consider (as is frequently done) stars as blackbodies, we may fit broad and narrow-band photometry from these objects with a Planck function, which will result in predictions for the object’s effective temperature, bolometric flux, and angular size. However, such an approximation is quite poor and overlooks many subtleties of stellar atmospheres, such as wavelength-dependent opacities.

In order to quantify the specifics of this example, a sample of 48 late giant stars from van Belle et al. (1999) that were well-characterized photometrically was examined with such an approximation. This sample has the benefit of having sizes measured and presented in van Belle et al. (1999) for comparison to the results obtained with the blackbody fit. A plot of the ratio of measured angular size to blackbody-derived angular size, as a function of the effective temperatures established for those stars in the paper, is shown in Figure 6. Errors in the blackbody angular size were derived from appropriate iteration of the Planck function within the errors specified for the photometry.

What is interesting to note in Figure 6 is the systematic offset of the ratios below a line of unity - the blackbody technique systematically delivers an angular size that is too large relative to the sizes that have been measured. The errors in that ratio, propagated from the blackbody and measured angular size errors, indicate that the ratio of unity is within most of the displayed error bars, as one would expect, but the general trend (on the order of $\sim 15\text{-}25\%$) shows that use of simple blackbody angular sizes could potentially bias interferometer calibrators.

As an example, if we were to use these sorts of stars in this manner with the Palomar Testbed Interferometer, we would find that for K -band operations with its 110-m baseline, we would need stars in the $\theta \leq 0.45 - 58$ mas range for use as absolute calibrators, given its limiting measurement precision of $(\sigma_{V^2})_{measured}=0.014$ (Boden et al. 1999) used in Equa-

tions 9 and 10 with a requirement for $r > 1$. Our previous CHARA Array example with $(\sigma_{V^2})_{measured}=0.020$ would require from this approach $\theta \leq 0.20$ mas, which would demand distant calibration objects beyond its sensitivity limits. Fortunately techniques have been developed with the apparent ability to predict stellar angular sizes to better than 10%, such as spectral energy distribution fitting (eg. Blackwell & Lynas-Gray (1994) and Cohen et al. (1999) agree with interferometric measures at the \sim few percent level), allowing for use of the very long baseline instruments such as the CHARA Array in an absolute fashion.

Clearly more sophisticated approaches to angular size estimation can be undertaken for interferometer calibrator stars, presumably with less susceptibility for size estimation bias, but the blackbody example is illustrative in how it demonstrates potential bias within an estimation technique. One of the most useful aspects of an astronomical interferometer, however, is its ability to mask bias in a calibrator size prediction technique for a sufficiently unresolved calibration source, and in doing so, deliver absolutely calibrated visibilities. Such an approach is not merely useful but essential to calibrate and verify predictive techniques of ever-increasing accuracy.

3. Taylor Series Bias in the Error Propagation Technique

The ‘routine propagation of errors’ given in Equation 4 is based upon just the first term of the Taylor series, which is subject to inaccuracies as the equation becomes more non-linear. This particular approximation is increasingly inaccurate for non-linear equations. Expanding upon our discussion of error propagation in §2.1 to probe the significance of the higher order terms, we may expand Equation 3 in a Taylor series about a given spatial frequency μ :

$$w(x|\mu) = w(\mu|\mu) + (x - \mu)w'(\mu|\mu) + \frac{(x - \mu)^2}{2!}w''(\mu|\mu) + \dots \quad (13)$$

The average of $w(x|\mu)$ can be written as

$$\overline{w(x|\mu)} = w(\mu|\mu) + \frac{\sigma_x^2}{2!}w''(\mu|\mu) + \dots \quad (14)$$

since, to first order, the $(x - \mu)w'(\mu|\mu)$ term drops out if x is centered around the mean μ . The usual error propagation presented in Equation 4 assumes the last term in Equation 14 is also negligible, which represents the Taylor series bias in the error propagation method:

$$bias_T = \overline{w(x|\mu)} - w(\mu|\mu) = \frac{\sigma_x^2}{2!}w''(\mu|\mu) \quad (15)$$

From Equations 3, 5 and 9, we may write this as

$$bias_T = \frac{\sigma_x^2}{2!} (8(jinc'(\mu))^2 - 8jinc(\mu)jinc''(\mu)) \quad (16)$$

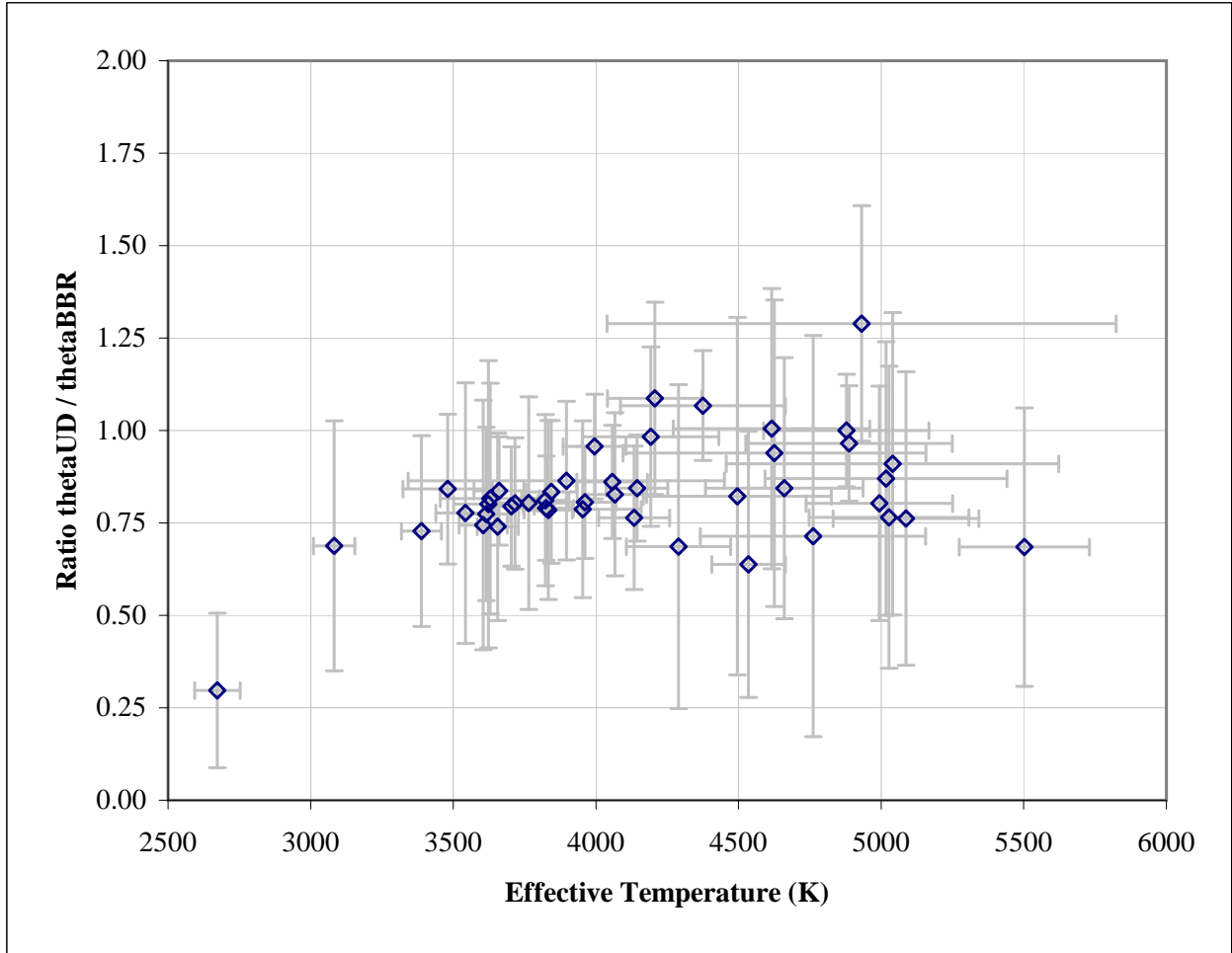


Fig. 6.— The ratio of measured angular size to predicted angular size (as derived from a blackbody approximation) as a function of effective temperature for 48 stars from van Belle et al. (1999).

Both $jinc$ and $jinc'$ are found in Equation 5, and a derivation of $jinc''$ may be referenced in the Appendix.

For most applications (including the examples given herein), σ_x is dominated by the uncertainty in predicted calibrator angular size, $(\sigma_\theta)_{predicted}$. As such, our example 5% error in θ means $\sigma_x = 5\% \times x$; the percentage bias as a function of calibrator predicted visibility ($bias_T(\mu)/V(\mu)^2$) is plotted in Figure 7 for our CHARA Array test case. The $bias_T$ term in this case starts to grow exponentially at $\theta \gtrsim 1.25$ mas; because of this, the ‘superresolved’ calibrator regime indicated in Figure 4 and discussed in §2.3 is undesirable for use as a source of calibrators.

4. Discussion

Predictive techniques are clearly imperfect - otherwise, why would we bother with measuring stellar angular sizes through V^2 measurements in the first place? As such, it is essential that work be carried out in the regime that is unaffected by potential bias in the calibrator angular size predictive technique, or bias from non-linearities in the visibility function.

Permutations upon the sample CHARA Array case in §2.2 are worth considering. While a 5% angular size prediction error is reasonable to expect for most calibration sources, for those sources with the very best *a priori* spectrophotometric characterization, a 2.5% prediction error may be possible. For this case, a 0.5% error in the knowledge of operational wavelength ($\sigma_\lambda = 0.01\mu\text{m}$ for K_s in Equation 8) still only contributes to the V^2 prediction error value by a factor of approximately ~ 1.02 ; prior angular size knowledge at the $<1\%$ level is necessary for this error term to contribute at a level greater than ~ 1.10 .

As the measurement precision increases (and $(\sigma_{V^2})_{measured}$ decreases), the unity crossing point seen in Figure 4 (where one passes from the absolute measurement regime into the relative measurement regime) decreases in value, ranging from ~ 0.62 mas for the case of 5% errors (typically associated with non-spatially filtered systems), down to ~ 0.40 mas for 1.5% errors (typical of systems with spatial filtering). This is rather intuitive: as one’s interferometric instrumentation improves in its ability to precisely measure visibilities, the degree to which that instrumentation is sensitive to potential biases in calibrator visibility prediction increases.

These values scale with spatial frequency, which itself will scale linearly with wavelength and baseline length for individual facilities. A selection of currently operational facilities is cited in Table 1, along with their relevant operational parameters of operational baseline, wavelength, and cited measurement precision. From these values, the maximum calibrator

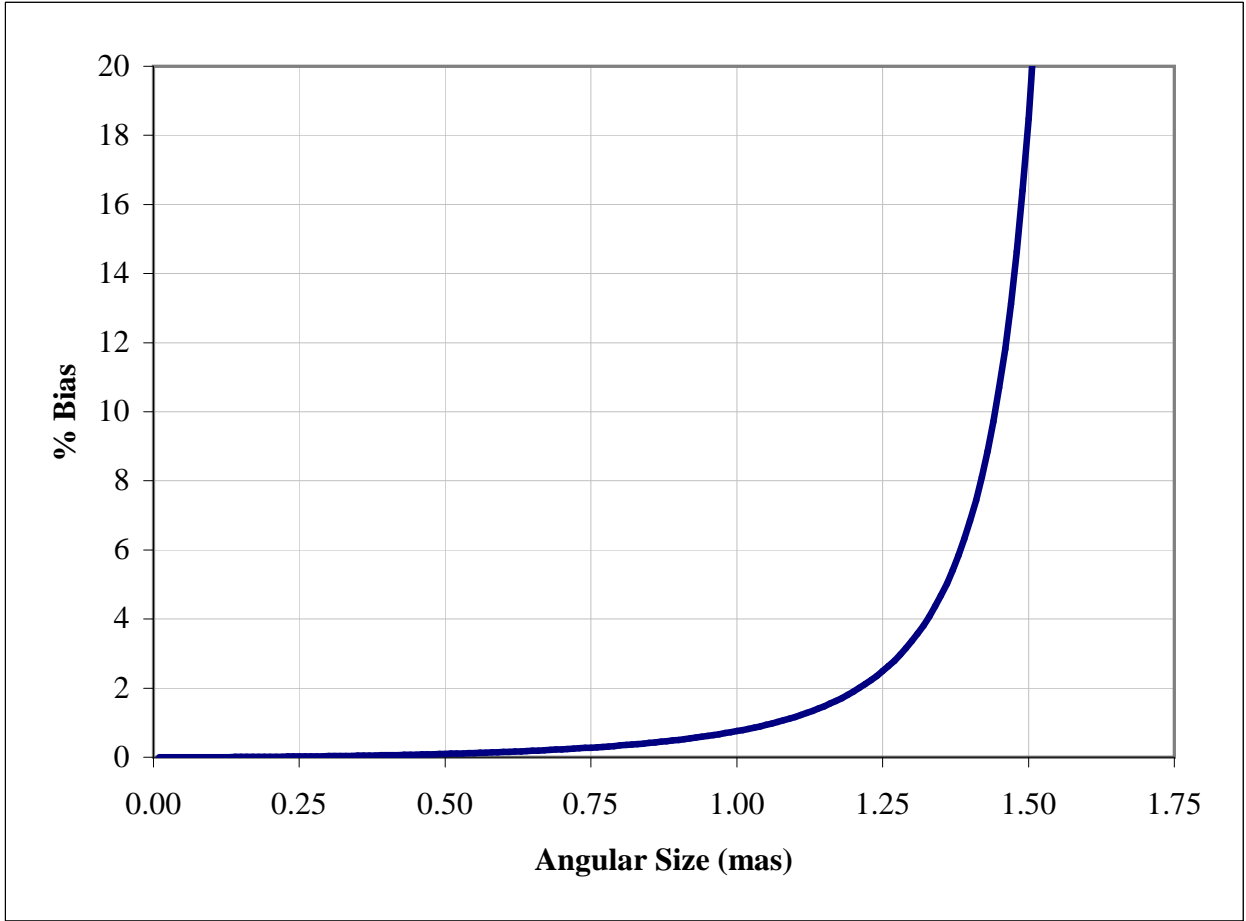


Fig. 7.— Percentage Taylor series bias in a V^2 measurement as discussed in §3 due to calibrator size prediction error of 5%, as a function of expected calibrator size.

angular size for absolute angular size measurements is derived using the process found in §2.3, assuming a 5% angular size estimation error.

5. Conclusion

Given the common use of optical and near-infrared interferometers to establish basic stellar parameters such as linear radius and effective temperature, it is of paramount importance to clearly understand the operational regime of one’s instrument as defined not only by its intrinsic capabilities, but also by the particulars of the observing technique. As shown in §2, in the case where resolved calibrators are being employed, the interferometric visibility measures provided are relative and as such are subject to biases - known and unknown - in the calibrator diameter estimation process employed.

The use of unresolved calibrators found in the regime as defined by the ratio test of Equation 10 is *essential* to making absolute measurements. Additionally, as seen in §3, the non-linear nature of the visibility function makes the routine propagation of errors incorrect for very low visibilities, and as such, biases the V^2 measurements as well.

We would like to thank Theo ten Brummelaar and Andy Boden for proofreading and thoughtful suggestions. This manuscript significantly benefited from the comments of an anonymous referee. Portions of this work were performed at the California Institute of Technology under contract with the National Aeronautics and Space Administration.

6. Appendix. Derivation of $jinc''(x)$

Starting with the two following Bessel function identities:

$$\frac{d}{dx}[x^m J_m(x)] = x^m J_{m-1}(x) \tag{17}$$

and

$$J_{-m}(x) = (-1)^m J_m(x), \tag{18}$$

we may use the recurrence relation

$$J_\nu(z) = \frac{2(\nu - 1)}{z} J_{\nu-1}(z) - J_{\nu-2}(z) \tag{19}$$

as applied to J_2 ,

$$J_2(z) = \frac{2}{z} J_1(z) - J_0(z), \tag{20}$$

and explicitly work out $jinc''(x)$:

$$jinc''(x) = \frac{d}{dx} jinc'(x) = \frac{d}{dx} \left(\frac{-J_2(x)}{x} \right) = \frac{d}{dx} \left[\frac{1}{x} \left(J_0(x) - \frac{2}{x} J_1(x) \right) \right] \quad (21)$$

$$= \left[\frac{-1}{x^2} \left(J_0(x) - \frac{2}{x} J_1(x) \right) \right] + \left[\frac{1}{x} \left(-J_1(x) + \frac{2}{x} J_2(x) \right) \right] \quad (22)$$

REFERENCES

- Airy, G. B. 1835, Trans. Camb. Phil. Soc., 5, 283
- Bessel, M. S. & Brett, J. M. 1988, PASP, 100, 1134
- Boden, A. F., et al. 1999, ApJ, 515, 356
- Born, M. & Wolf, E. 1980, Oxford: Pergamon Press, 1980, 6th corrected ed.
- Blackwell, D. E. & Lynas-Gray, A. E. 1994, A&A, 282, 899
- Bracewell, R. N. 2000, The Fourier transform and its applications / Ronald N. Bracewell. Boston : McGraw Hill, c2000. (McGraw-Hill series in electrical and computer engineering. Circuits and systems)
- Cohen, M., Witteborn, F. C., Carbon, D. F., Davies, J. K., Wooden, D. H., & Bregman, J. D. 1996, AJ, 112, 2274
- Cohen, M., Walker, R. G., Carter, B., Hammersley, P., Kidger, M., & Noguchi, K. 1999, AJ, 117, 1864
- Colavita, M. M. 1999, PASP, 111, 111
- di Benedetto, G. P. 1993, A&A, 270, 315
- Dyck, H. M., Benson, J. A., & Ridgway, S. T. 1993, PASP, 105, 610
- Domiciano de Souza, A., Kervella, P., Jankov, S., Abe, L., Vakili, F., di Folco, E., & Paresce, F. 2003, A&A, 407, L47
- Dyck, H. M., Benson, J. A., van Belle, G. T., & Ridgway, S. T. 1996, AJ, 111, 1705
- Hajian, A. R., et al. 1998, ApJ, 496, 484

- Kervella, P., Thévenin, F., Ségransan, D., Berthomieu, G., Lopez, B., Morel, P., & Provost, J. 2003, *A&A*, 404, 1087
- Millan-Gabet, R., Pedretti, E., Monnier, J. D., Schloerb, F. P., Traub, W. A., Carleton, N. P., Lacasse, M. G., & Segransan, D. 2005, *ApJ*, 620, 961
- Mozurkewich, D., et al. 1991, *AJ*, 101, 2207
- ten Brummelaar, T., et al. 2005, *ApJ*, accepted
- Tycner, C., et al. 2004, *AJ*, 127, 1194
- van Belle, G. T. 1999, *PASP*, 111, 1515
- van Belle, G. T., et al. 1999, *AJ*, 117, 521
- van Belle, G. T., et al. 2005, *ApJ*, submitted

Table 1. Maximum calibrator sizes for absolute calibration of V^2 measurements for a variety of current interferometric facilities, assuming 5% calibrator size estimate errors.

Facility	Maximum Baseline (m)	Band	Cited V^2 Meas. Error	Maximum calibrator size (mas)	Notes	
CHARA	330	K	0.04	0.77	No spatial filtering	van Bel
CHARA	330	K	0.02	0.45	Spatial filtering	Under c
IOTA	38	J	0.046	2.3	No spatial filtering	Millan-
NPOI	37.5	V	0.02	1.0	No spatial filtering	Tycner
PTI	110	K	0.014	1.1	Spatial filtering	Boden c
VLTI	187	K	0.004	0.31	Spatial filtering, photometric monitoring	Kervella